

ARMY RESEARCH LABORATORY



Finite Element Modeling and Analysis of an M855 Cartridge

by Joseph T. South and Larry W. Burton

ARL-TR-3301

September 2004

NOTICES

Disclaimers

The findings in this report are not to be construed as an official Department of the Army position unless so designated by other authorized documents.

Citation of manufacturer's or trade names does not constitute an official endorsement or approval of the use thereof.

DESTRUCTION NOTICE—Destroy this report when it is no longer needed. Do not return it to the originator.

Army Research Laboratory

Aberdeen Proving Ground, MD 21005-5069

ARL-TR-3301**September 2004**

Finite Element Modeling and Analysis of an M855 Cartridge

Joseph T. South and Larry W. Burton
Weapons and Materials Research Directorate, ARL

REPORT DOCUMENTATION PAGE				Form Approved OMB No. 0704-0188	
<p>Public reporting burden for this collection of information is estimated to average 1 hour per response, including the time for reviewing instructions, searching existing data sources, gathering and maintaining the data needed, and completing and reviewing the collection information. Send comments regarding this burden estimate or any other aspect of this collection of information, including suggestions for reducing the burden, to Department of Defense, Washington Headquarters Services, Directorate for Information Operations and Reports (0704-0188), 1215 Jefferson Davis Highway, Suite 1204, Arlington, VA 22202-4302. Respondents should be aware that notwithstanding any other provision of law, no person shall be subject to any penalty for failing to comply with a collection of information if it does not display a currently valid OMB control number.</p> <p>PLEASE DO NOT RETURN YOUR FORM TO THE ABOVE ADDRESS.</p>					
1. REPORT DATE (DD-MM-YYYY) September 2004		2. REPORT TYPE Final		3. DATES COVERED (From - To) November 2002 to May 2003	
4. TITLE AND SUBTITLE Finite Element Modeling and Analysis of an M855 Cartridge				5a. CONTRACT NUMBER	
				5b. GRANT NUMBER	
				5c. PROGRAM ELEMENT NUMBER	
6. AUTHOR(S) Joseph T. South and Larry W. Burton (both of ARL)				5d. PROJECT NUMBER 622618.H80	
				5e. TASK NUMBER	
				5f. WORK UNIT NUMBER	
7. PERFORMING ORGANIZATION NAME(S) AND ADDRESS(ES) U.S. Army Research Laboratory Weapons and Materials Research Directorate Aberdeen Proving Ground, MD 21005-5069				8. PERFORMING ORGANIZATION REPORT NUMBER ARL-TR-3301	
9. SPONSORING/MONITORING AGENCY NAME(S) AND ADDRESS(ES)				10. SPONSOR/MONITOR'S ACRONYM(S)	
				11. SPONSOR/MONITOR'S REPORT NUMBER(S)	
12. DISTRIBUTION/AVAILABILITY STATEMENT Approved for public release; distribution is unlimited.					
13. SUPPLEMENTARY NOTES					
14. ABSTRACT A finite element model of an M855 brass cartridge inside an M16A4 barrel has been generated. The goal of the research was to develop and validate a baseline mechanical model for a brass M855 cartridge during realistic firing conditions. This model incorporates the strength changes in the cartridge attributable to the variation in the hardness and microstructure produced during manufacturing. The results of the model are used to evaluate the stress, strains, and resulting deformation that a brass cartridge case undergoes during ignition. The model predicts a stress state within the brass that demonstrates a 1.8 factor of safety. The results were validated with experimental measurements from expended M855 cartridges and showed good correlation with the predicted plastic deformation of the model. The creation of the validated model serves as a platform from which alternate lightweight materials for the cartridge case can be evaluated analytically.					
15. SUBJECT TERMS brass; cartridge; finite element; M855					
16. SECURITY CLASSIFICATION OF:			17. LIMITATION OF ABSTRACT UL	18. NUMBER OF PAGES 25	19a. NAME OF RESPONSIBLE PERSON Joseph T. South
a. REPORT Unclassified	b. ABSTRACT Unclassified	c. THIS PAGE Unclassified			19b. TELEPHONE NUMBER (Include area code) 410-306-0763

Standard Form 298 (Rev. 8/98)

Prescribed by ANSI Std. Z39.18

Contents

List of Figures	iv
List of Tables	iv
1. Introduction	1
2. Approach	1
3. Material Input and Model Generation	3
3.1 Material Properties	3
3.2 Finite Element Model Mesh	6
3.3 Applied Load	7
3.4 Applied Boundary Conditions	9
3.5 Solution Control	10
4. Results	10
4.1 Model Validation	15
5. Summary	16
6. References	17
Distribution List	18

List of Figures

Figure 1. CAD drawing of an M855 cartridge inside the chamber of an M16A2. (The unsupported region of the cartridge is shown in the inset.)	2
Figure 2. Complete 2-D axisymmetric FEA brass cartridge model showing all components.....	3
Figure 3. Hardness gradient for an M855 brass cartridge (<i>I</i>).	4
Figure 4. Stress-strain tensile data for 70-30 alpha brass at different levels of cold rolling, recrystallization, and re-rolling	5
Figure 5. Compressive stress-strain curve for cartridge brass.	6
Figure 6. Chamber and projectile base pressure for an M855 cartridge.....	8
Figure 7. Plot of the internal pressure gradient in Pascals applied to the M855 cartridge.	8
Figure 8. Applied boundary conditions.	9
Figure 9. Predicted mid-thickness stresses along the length of the cartridge.	11
Figure 10. Plot of the Von Mises stress state in Pascals in the neck and shoulder region of the cartridge at maximum ballistic pressure.	11
Figure 11. Predicted mid-thickness strain along the length of the cartridge.	12
Figure 12. Predicted mid-thickness failure criteria along the length of the cartridge.....	12
Figure 13. Plot of the axial stresses in pascals near the extractor groove.....	13
Figure 14. Plot of the Von Mises factor of safety for the brass cartridge.....	13
Figure 15. Predicted versus the measured radial plastic deformation along the length of the cartridge.	16

List of Tables

Table 1. Results of varying levels of cold rolling, recrystallization and re-rolling on the hardness and modulus of 70-30 alpha brass (4,5).	4
--	---

1. Introduction

The use of brass for cartridge cases has a long history and is particularly embedded into the culture of ammunition for small arms. For more than 100 years, brass has served adequately and admirably as a material for cartridge cases. Its relatively high strength and ductility provide it with the twofold ability to withstand large rupture pressures while undergoing deformations that provide the means to seal combustion gases in the chamber. These properties have made brass the intuitively obvious material of choice for cartridge applications.

However, more recently, interest in ammunition weight reduction has increased and therefore, investigations into materials other than the high-density brass have arisen. In order to adequately assess alternate lightweight materials for cartridges, it is first necessary to understand the performance of brass in this role. It was with this thought that an effort was undertaken to employ modern finite element techniques to represent the behavior of brass cartridges.

Interestingly enough, despite the long history of brass usage, little information was found in the literature that reported about the mechanical properties of “cartridge brass,” a copper alloy composed of 70% copper and 30% zinc. This report details the literature findings and specifies those extrapolations that were required to provide a complete characterization of the material over the full range of strains encountered.

The over-arching goal of this exercise was to establish a modeling technique for cartridge cases, which could be validated against the limited data available during realistic firing conditions. The M855 brass cartridge in an M16A4 barrel was selected for this purpose. The results of the model are used to evaluate the stress, strains, and resulting deformation that a brass cartridge case undergoes during operation. The technique was validated by experimental measurements from expended M855 cartridges. With this baseline, the technique can be used to assess other materials and geometries and investigate the influence of temperature, pressure, and firing rate. It is the authors’ intent for this to be the first in a series of reports that investigate these various parameters.

2. Approach

A finite element model was constructed that included the brass cartridge with primer inside the chamber of an M16A2 rifle. The geometry of the cartridge, primer, barrel, barrel extension and bolt was obtained from the manufacturer’s drawings (1,2). The drawings were entered into computer-aided design (CAD) software so that they could be made proportional and for application of the tolerances. The conceptual dimensions of all the components were used.

A cutaway CAD drawing of an M855 cartridge set inside the chamber is shown in figure 1. In the figure, the cartridge is shown in intimate contact with the chamber wall. Included in the figure is the barrel extension. One feature to note is the length of the unsupported region near the head of the cartridge. This unsupported region is necessary to allow for the motion of the bolt and the engagement of the extractor pin with the extractor grooves.

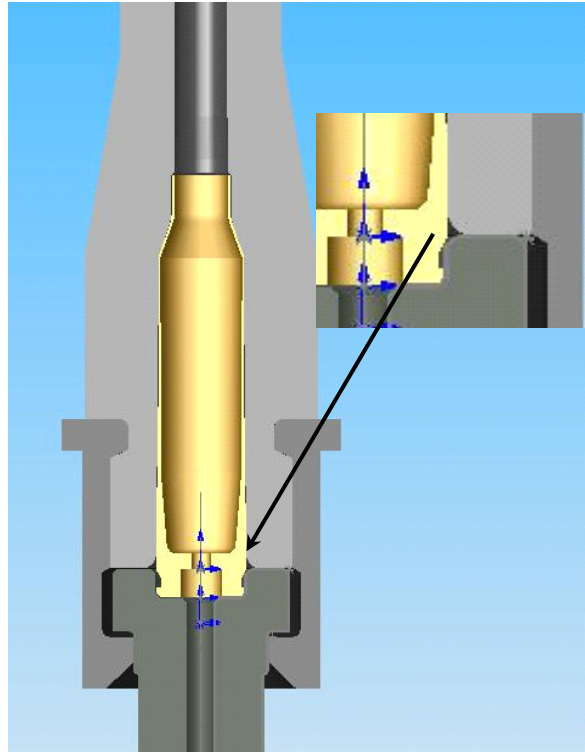


Figure 1. CAD drawing of an M855 cartridge inside the chamber of an M16A2. (The unsupported region of the cartridge is shown in the inset.)

The translation from the CAD drawing to the finite element analysis (FEA) model is shown in figure 2. Consistent with the nature of the problem, symmetry was employed to reduce the model from a full three-dimensional (3-D) analysis to a two-dimensional (2-D) axisymmetric analysis to reduce the computation time. The cartridge was considered to reside fully inside the chamber region so that the shoulder of the cartridge and the surface of the chamber were in contact.

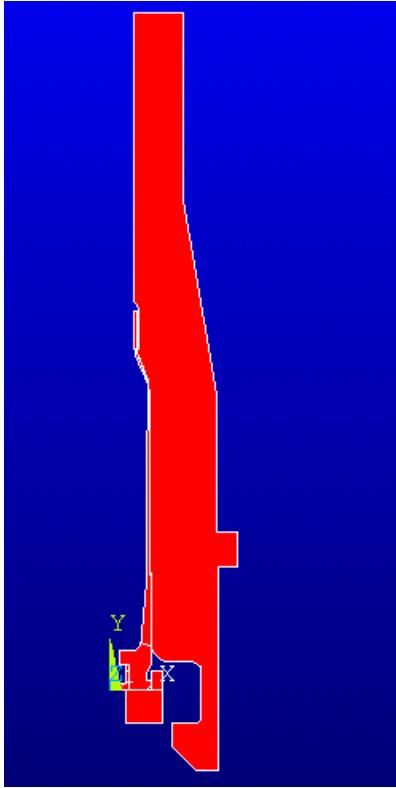


Figure 2. Complete 2-D axisymmetric FEA brass cartridge model showing all components.

3. Material Input and Model Generation

In order to develop an accurate model, realistic material properties and boundary conditions that mimic the actual cartridge and operating conditions were required. This information was obtained through experimental data and an empirical approach.

3.1 Material Properties

During the numerous drawing and annealing steps that occur during the manufacturing of a brass cartridge, a hardness and microstructure gradient exists along the length (3). This gradient is produced so that the highest hardness within the case occurs at the unsupported region of the cartridge. The lowest hardness occurs in the neck region to allow for bullet crimping and detachment from the cartridge during firing. This hardness profile from the M855 technical drawing is shown in figure 3. The plot shows the minimum and maximum allowable Vickers hardness from a 2.5-kg load.

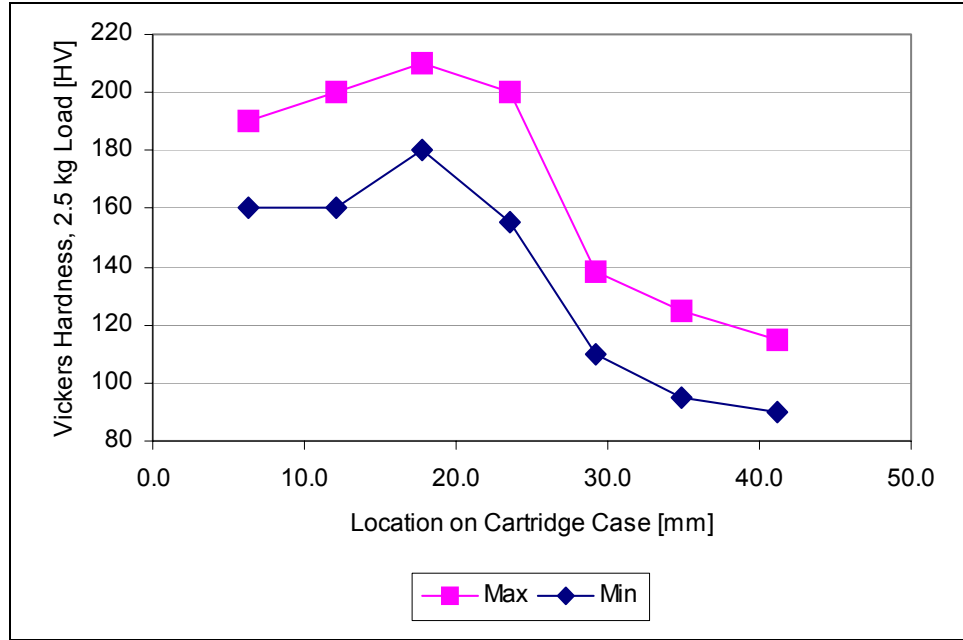


Figure 3. Hardness gradient for an M855 brass cartridge (1).

In order to correctly model the response of the M855 cartridge, this hardness gradient must be properly represented. The research of Yang (4,5) was used to correlate the hardness values with a stress strain curve. In this work, Yang measured both the tensile response of 70-30 alpha brass¹ and the diamond pyramid hardness after varying levels of cold rolling² and recrystallization. The strain rate in the elastic region was $3.3 \times 10^{-4} \text{ sec}^{-1}$. Yang found that the tensile properties and the hardness increased as the amount of re-rolling and recrystallization increased. Table 1 shows the data from Yang.

Table 1. Results of varying levels of cold rolling, recrystallization and re-rolling on the hardness and modulus of 70-30 alpha brass (4,5).

Processing	Hardness (HV)	Modulus (GPa)
60% Cold rolled	185	63.4
60% Cold rolled 48% recrystallized 30% re-rolled	195	63.4
60% Cold rolled 48% recrystallized 20% re-rolled	175	59.8
60% Cold rolled 48% recrystallized 10% re-rolled	155	47.5
Fabricated	100	47.5
Olin, soft brass		47.9

The data presented by Yang did not go below a hardness value (HV) of 160; however, hardness values in the neck and shoulder region of the cartridge average 100 HV. We established data for

¹Alpha brass containing as much as 36% of zinc is usually the single alpha phase with good cold working properties; 70-30 alpha brass means 70% copper and 30% zinc.

²Cold rolling is a process whereby the material is deformed by rolling at relatively low temperatures.

the 100-HV point by interpolating the stress-strain data from Yang and applying an interpolated stress-strain curve that followed the same trends. All the curves correlating to data in table 1 are presented in figure 4. These tensile data agree with those in other literature (3,6,7). Included in the table are tensile data obtained from cartridge manufacturer Olin-Winchester (8). The hardness of the material is unknown, but the manufacturer considered the brass to be soft. The engineering tensile strength of the brass was 306 MPa, which is roughly the same as completely annealed brass (9) at 317 MPa. Given that the neck and the shoulder of the cartridge undergo some cold working during the punch and drawing processes and then are only partially annealed, it was assumed that the fabricated curve was a reasonable representation of the material in this region. The stress-strain curve possessed the same trend as the experimental data of Yang but had lower yield strength.

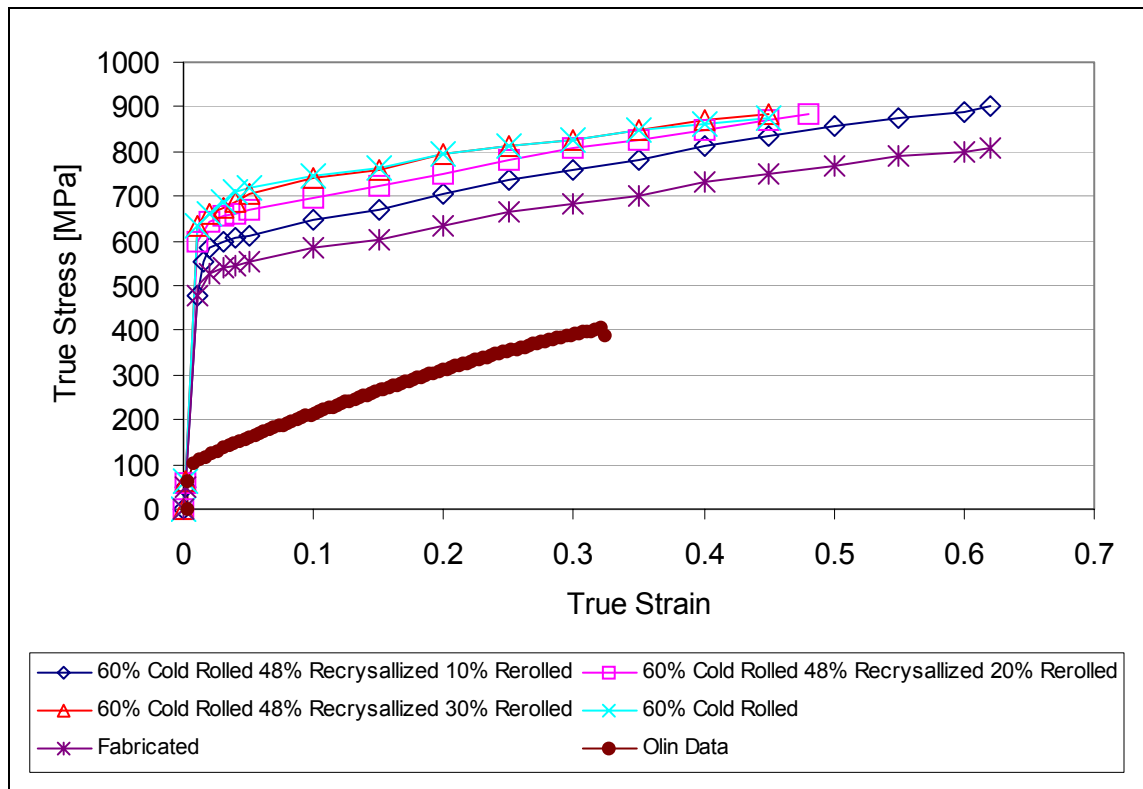


Figure 4. Stress-strain tensile data for 70-30 alpha brass at different levels of cold rolling, recrystallization, and re-rolling.

The hardness gradient within the brass cartridge was captured in the FEA model by the stress-strain curves in figure 4. For modeling purposes, the cartridge was sectioned into three areas: head, body, and neck/shoulder, as shown in figure 2. Each of the three regions was associated with an appropriate stress-strain curve. The curves had the representative hardness values of 185, 155, and 100 HV correlating to the 60% cold rolled, 60% cold rolled, 48% recrystallized, 10% re-rolled and the fabricated curves, respectively. Poisson's ratio for each brass was set to 0.35.

The barrel and barrel extension were assumed to be linear elastic steel with a modulus of 200 GPa and Poisson's ratio of 0.3. No material properties were available for the primer. It was assumed that the primer possesses the same structural characteristics as the head region of the cartridge, with a hardness of 185 HV. The overall FEA model geometry consisted of five different areas and four different material properties.

The input to the FEA model was solely the tensile response. It was assumed that the brass exhibited a homogeneous isotropic response and has an identical response in compression. To verify this response, the compressive stress-strain data for cartridge brass were obtained (10). The compressive stress-strain curve is presented as figure 5, which shows the maximum compressive stress to be approximately 600 MPa at a true strain of 0.5. The hardness of the material is unknown. Assuming that the brass behaves as a homogeneous isotropic material, this compressive stress-strain curve would put the hardness of the brass between the fabricated and Olin data of figure 4. This would make the curve that of a half hard brass (9). This is a reasonable assumption since the data do not indicate any pre-treatment of the material such as cold rolling or annealing. The assumption of brass behaving as a homogeneous isotropic material was carried through the remainder of the modeling effort. With the geometry and the material properties established, the next step was to mesh the model.

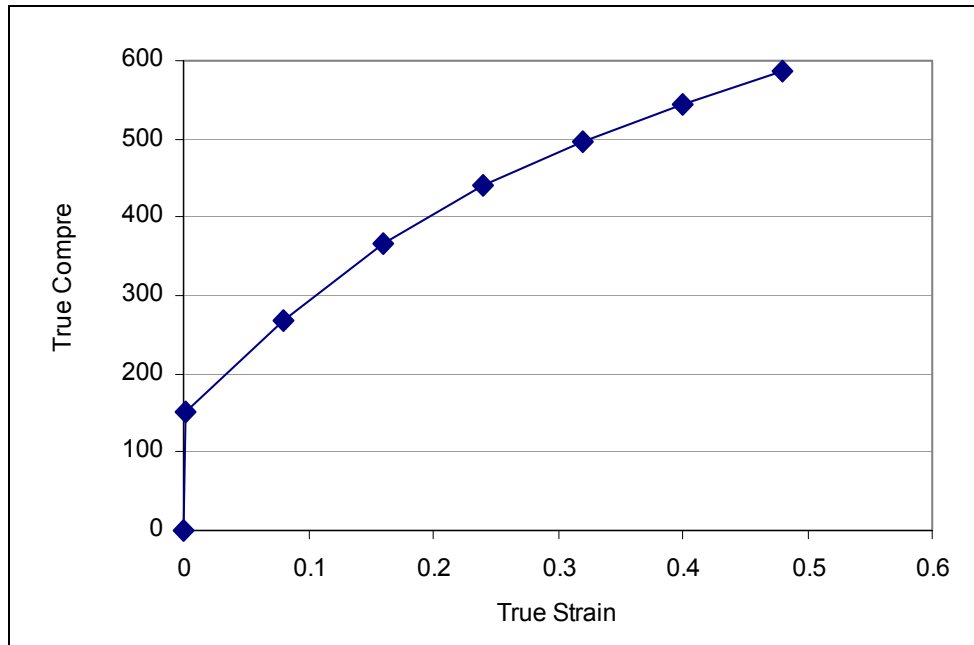


Figure 5. Compressive stress-strain curve for cartridge brass.

3.2 Finite Element Model Mesh

The areas of the model were meshed with the plane 82 ANSYS³ element. This is an eight-noded 2-D element with plasticity and axisymmetric capability. The axis of symmetry was the y-axis.

³ANSYS®, which is not an acronym, is a registered trademark of ANSYS, Inc.

All four materials (the steel and three different brasses) were modeled with isotropic linear elastic properties. Plasticity of the brass was modeled with the isotropic Mises (11) plasticity model. To use this model, the entire stress-strain curve for each respective brass was entered. Given that the stress-strain curves were in true stress and strain units, the large displacement option was invoked. This option requires that all input be in true stress and strain and output of the results be expressed similarly.

Contact pairs were added to model the interaction along the cartridge-chamber wall and the cartridge-primer interfaces. The contact pair between the cartridge and the chamber allowed for the expansion of the cartridge against the chamber during the combustion event. The pair between the cartridge and the primer modeled the interaction of the interface as well as provided the ability to have the primer to be press fit into the cartridge. ANSYS models contact pairs by allowing the user to specify a target and a contact surface. We modeled the interference fit between the primer and the cartridge by providing an offset to the contact surface so that the contact and target surfaces of the pair were in a mathematical penetration. This penetration resulted in a compression fit of the primer cup into the head of the cartridge case.

3.3 Applied Load

Load was applied to the model as an internal pressure obtained from experimental measurements (12). The pressure at the base of the projectile was calculated with the Lagrangian correction for the pressure gradient down the bore (13). This relation is shown as equation 1.

$$P_b = \frac{P_c}{1 + \frac{c}{2M_p}}, \quad (1)$$

in which P_c is the pressure in the chamber, P_b is the pressure at the base of the projectile, c is the mass of the charge, and M_p is the mass of the projectile. The calculated base pressure and the experimentally obtained chamber pressure applied in the FEA model are plotted in figure 6.

It was assumed that the pressure in the primer cavity was less than the maximum chamber pressure because of the short duration of the pulse. As a result, the pressure in the primer cavity was chosen to be the same as the base pressure in figure 6. The meshed model of the cartridge showing the applied maximum pressure loading is presented in figure 7.

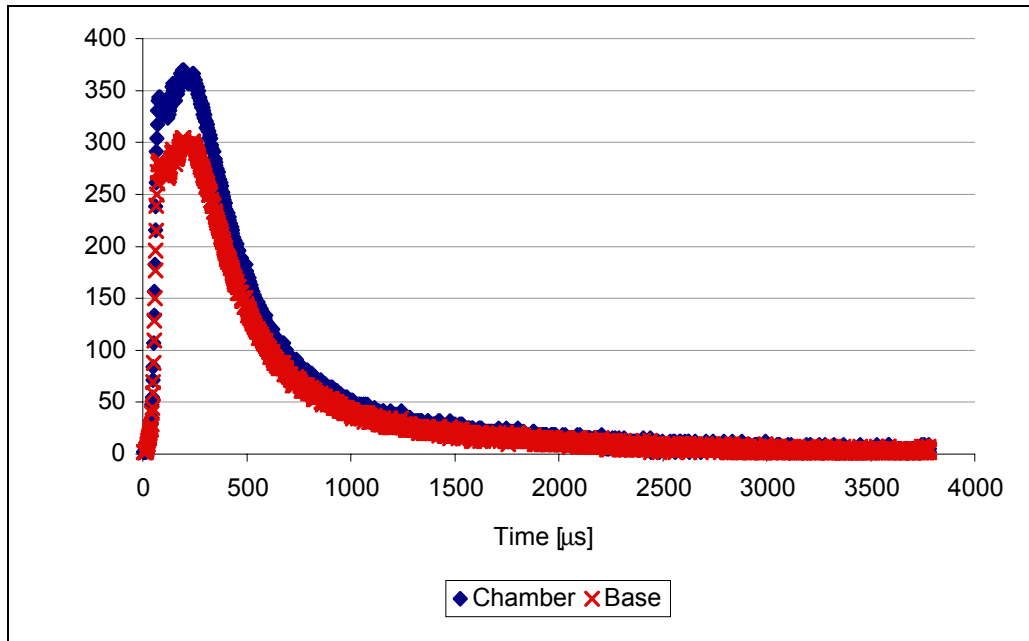


Figure 6. Chamber and projectile base pressure for an M855 cartridge.

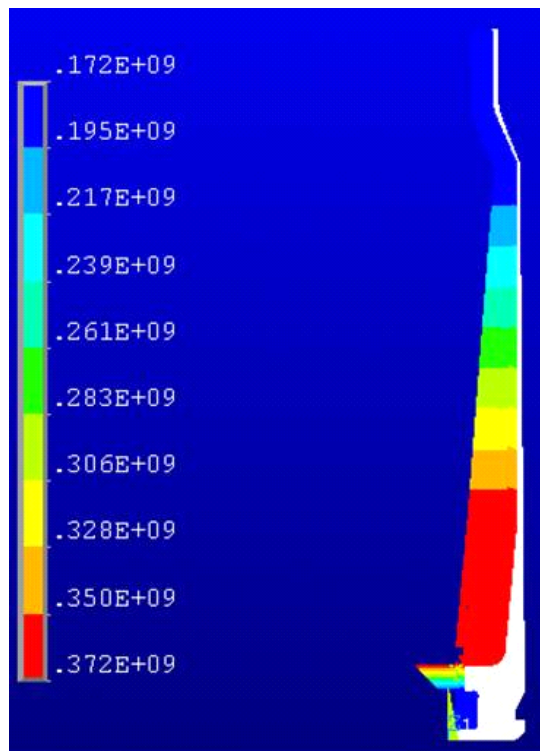
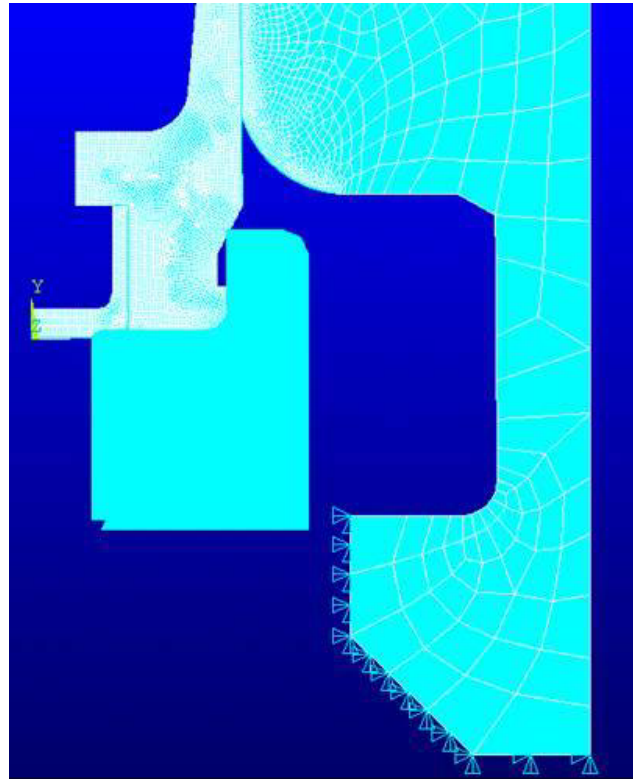


Figure 7. Plot of the internal pressure gradient in Pascals applied to the M855 cartridge.

Boundary conditions were applied to realistically constrain the model. Axisymmetric boundary conditions were applied to the inside primer wall. In order to fix the barrel in space, a zero displacement constraint, in both the x and y directions, was applied to the end of the barrel extension.

A new boundary condition was created that accounted for this rearward motion. An axisymmetric representation of the bolt face was incorporated into the model to more closely represent realistic conditions. The dimensions of the bolt were obtained from the 3-D technical data package (TDP) for the M16A2 (14). A gap of 12.8 μm separating the faces of the cartridge and the primer cup from the bolt face was set. This distance allowed for some finite separation at the head of the cartridge. To model the interaction between these faces, two additional contact pairs were added: one pair for the cartridge-bolt interaction and one pair for the primer-bolt interaction. To finish the boundary conditions, a symmetric boundary condition was applied to the bolt's inner wall and zero displacement conditions were applied to the remaining free faces of the bolt. The applied boundary conditions and added bolt feature are presented in figure 8.



9

3.5 Solution Control

The finite element model was solved as a 2-D axisymmetric static model with large displacement effects. The large displacement effects were used since all the data for the cartridge brass were in terms of true stress and strain. To facilitate convergence, the internal pressure load curves of figure 6 were broken into 22 separate loading steps. Automatic time stepping was employed to decrease the running time of the model. Initial loads on the model resulting from the contact pairs were linearly increased in order to achieve convergence.

4. Results

The finite element model was post-processed to obtain the stress and strain through the mid-thickness of the cartridge at the peak pressure as well as the plastic displacement that occurred because of the applied load. Generalized stress plots were produced to determine the areas of high stress generated during the peak internal pressure. A maximum stress failure criterion was chosen to determine the relative distance from failure. The equation is

$$F.C. = \frac{\sigma_{Ultimate}}{\sigma} > 1 \quad (2)$$

in which $\sigma_{Ultimate}$ is the ultimate tensile strength and σ is the stress in the system. For cases when the stress was negative, the ultimate compressive strength was used. Failure is assumed to occur when the failure criterion equals unity. The factor of safety that existed within the cartridge because of the applied load was determined by the equation

$$F.S. = \frac{\sigma_{Allowed}}{\sigma_{Applied}} > 1 \quad (3)$$

in which $\sigma_{Allowed}$ is the maximum allowable stress and $\sigma_{Applied}$ is the stress in the system. We obtained the stress and strain through the thickness of the cartridge by plotting a nodal path midway through the thickness of the cartridge from the head to the neck. The stress and strains were evaluated for failure at the maximum applied internal pressure. This loading coincided with load step 12 in the model. The results at this load level are presented in figures 9 through 14.

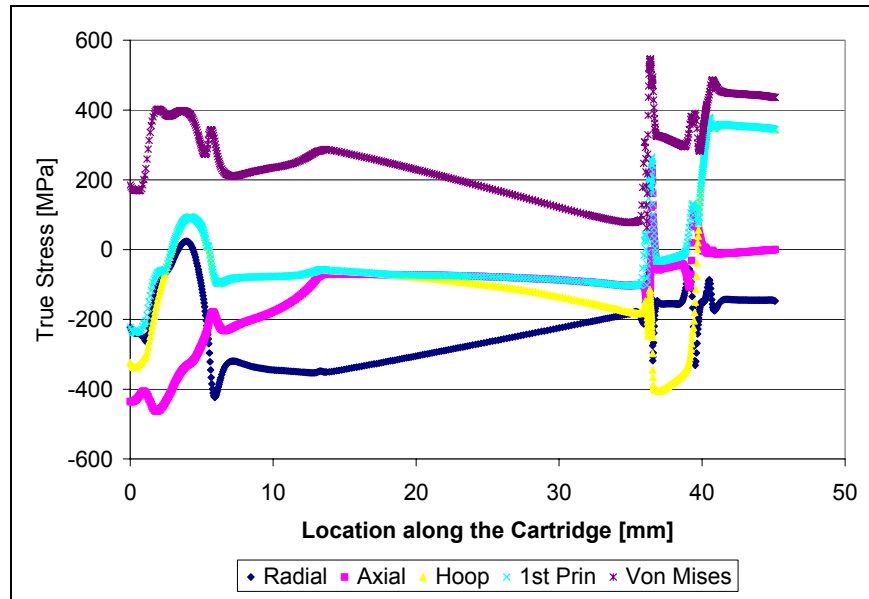


Figure 9. Predicted mid-thickness stresses along the length of the cartridge.

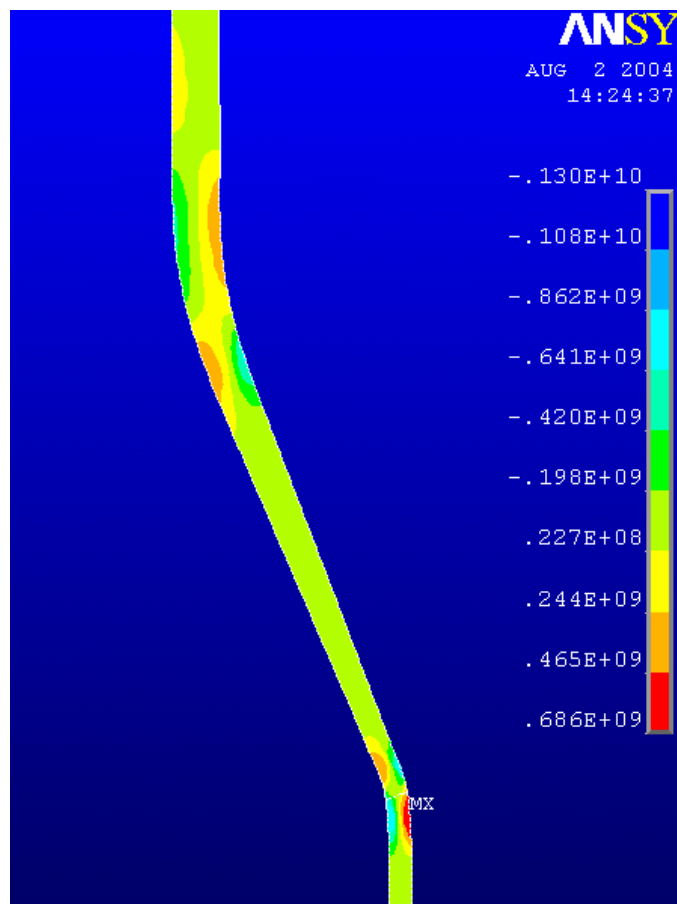


Figure 10. Plot of the Von Mises stress state in pascals in the neck and shoulder region of the cartridge at maximum ballistic pressure.

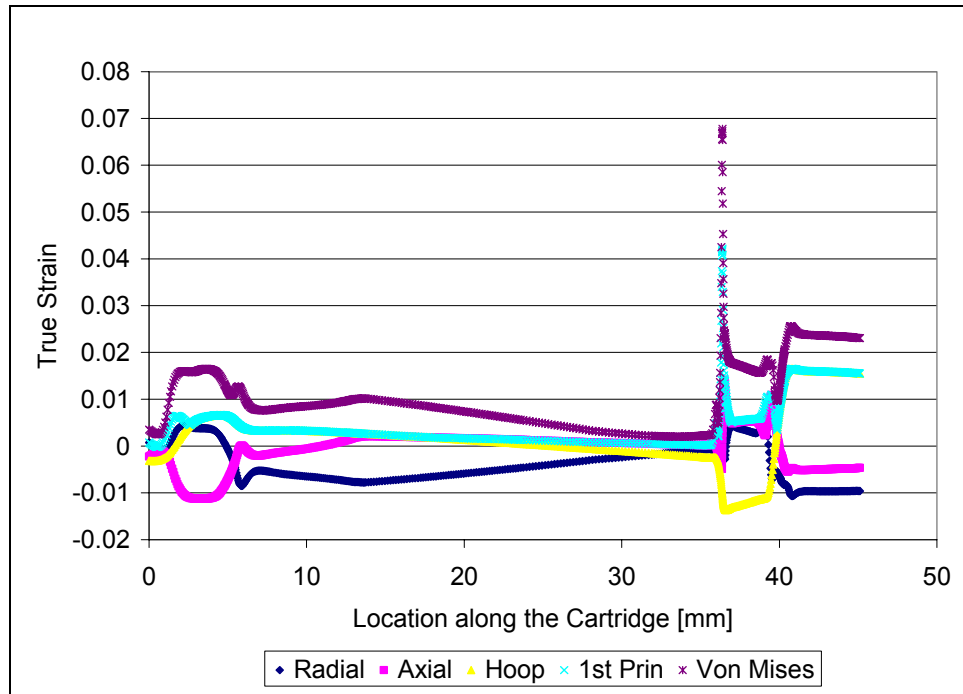


Figure 11. Predicted mid-thickness strain along the length of the cartridge.

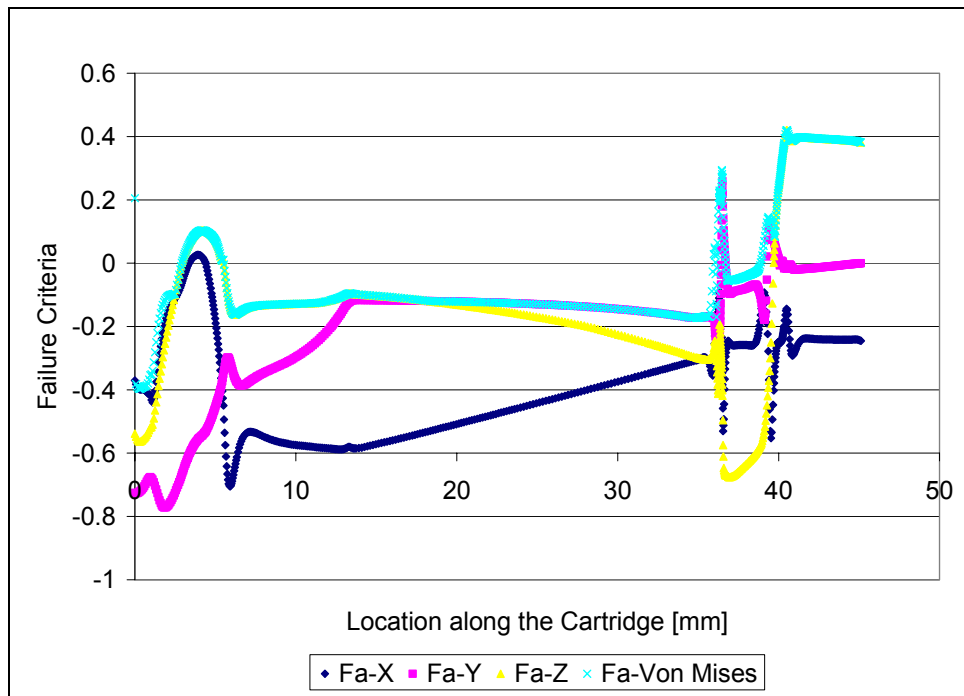


Figure 12. Predicted mid-thickness failure criteria along the length of the cartridge.

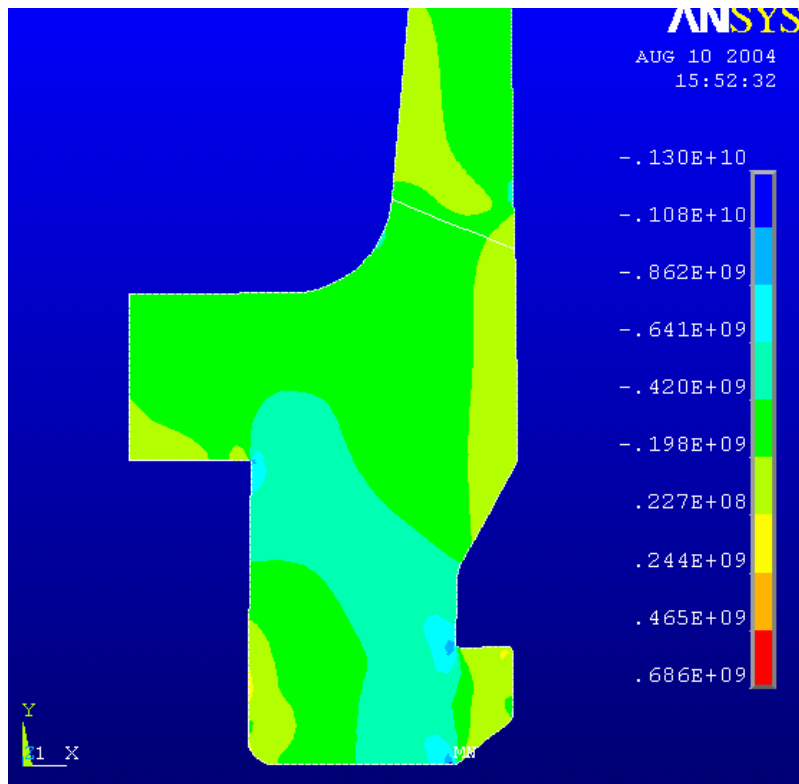


Figure 13. Plot of the axial stresses in pascals near the extractor groove.

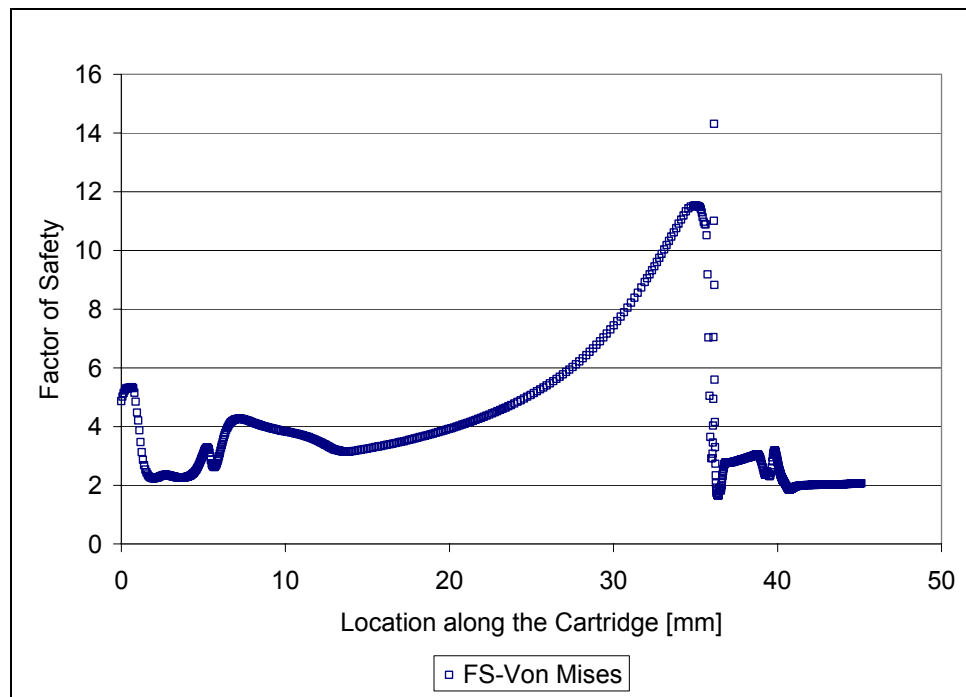


Figure 14. Plot of the Von Mises factor of safety for the brass cartridge.

The predicted true stresses through the mid-thickness of the cartridge wall are presented in figure 9. The radial, axial, and hoop stresses are largely compressive. This stress state is attributable to the expansion of the cartridge against the chamber wall during pressurization as well as the rearward movement of the cartridge during firing. The transition from the unsupported region of the cartridge (figure 1) to the supported is marked by the stress redistribution from a tensile stress to a compressive stress in all three components between 4 and 6 mm. The triaxial stress state remains compressive until the onset of the shoulder in the cartridge at roughly 36 mm from the base. At this location, the triaxial stress state becomes rather complex because of bending within the cartridge to conform to the chamber dimensions. The outer diameter (OD) of the cartridge is in compression while the interior diameter (ID) of the cartridge is in tension. This stress state is shown in figure 10. Between the onset of the shoulder and the onset of the neck, the cartridge is in a triaxial state of compression. At the onset of the shoulder, a bending of the cartridge occurs again. The stress state within these bending regions results in spikes within the mid-thickness plots of figures 9 and 11. These spikes are an artifact of post-processing the model as the nodal path used to produce the curves overlaps these complex stress states and the points are interpolated from the model results.

Within the neck of the cartridge, the brass is in compression in the radial and axial directions; however, the cartridge undergoes a tensile load in the hoop direction. This tensile load is a result of a nominal gap between the cartridge and the chamber ID of 71 μm . The magnitude of this gap is discussed in section 4.1 in relation to the experimental verification of this modeling.

The mid-thickness strains are presented in figure 11. The results complement those of figure 9 with the triaxial strain state following the same pattern as the stresses. The spike in the strain plot at 36 mm is an artifact of the nodal path. The maximum strain obtained with the cartridge occurs in the neck region with a Von Mises strain of 2.5%. The high strains that occur in this area will be exploited in the experimental validation of the model.

The failure criterion of equation 2, which is plotted in figure 12, was calculated so that if a stress component were compressive, it would be evaluated against the compressive strength of figure 5, and if a stress component were tensile, it would be evaluated against the tensile strength of figure 4. The maximum strength failure criteria of equation 2 show that the cartridge's axial stresses approach 76% of their ultimate, 2 mm from the base. This location corresponds to the extractor groove in the cartridge. Axial stresses are highly compressive because of a combination of the reduction in radius to accommodate the extractor and the cartridge being forced rearward during firing against a stationary bolt face. A graphic of these stresses near the extractor groove is presented as figure 13. The failure criterion achieves the highest tensile values at 40% of ultimate in the neck of the overall cartridge.

The factor of safety of the brass cartridge is presented in figure 14. Because of the complex stress state within the cartridge, only the Von Mises stress was evaluated to calculate the factor of safety. The factor of safety varied along the length of the cartridge, achieving a maximum

11.5 before the onset of the neck of the cartridge. The minimum factor of safety observed within the cartridge was 1.8 which occurred within the bending region of the neck.

4.1 Model Validation

The modeling effort evaluated the stress and strains within the cartridge and compared them to criteria to evaluate their acceptability. In order to validate the model, the numerical results were compared to measurements from expended cartridges. With the model, sensitivity analysis was performed to determine the effect of the tolerances on the response of the brass cartridge. Two FEA models were created: one with a minimum cartridge OD to maximum chamber ID tolerance (maximum clearance) and one with a maximum cartridge OD to minimum chamber ID tolerance (minimum clearance). The models were evaluated with the previously discussed approach, and the predicted radial plastic deformation in the cartridge was evaluated. Fourteen expended brass cartridges were measured to determine their change in radius in the neck because of firing. The firing history of the measured cartridges was unknown but their manufacture stamp linked them to production at Lake City Army Ammunition Plant, Independence, Missouri, in 1989. The change in the radius of the cartridges was evaluated from the ideal cartridge dimension.

Figure 15 shows the results of the sensitivity analysis. The measured radial displacement from the expended cartridges falls between the minimum and maximum bore tolerances. The onset of the plastic deformation coincides with the shoulder region of the cartridge. Increasing the bore diameter increases the magnitude of the plastic deformation and shifts the onset of that deformation rearward toward the base of the cartridge. There is a minor amount of predicted plastic deformation near the end of the unsupported region, 6 and 7 mm from the base. The magnitude of these values was approximately 1 μm . These magnitudes could not be accurately measured on the expended cartridge because of the taper of the cartridge OD and the generic location of the prediction. The most accurate and reliable measurements could only be obtained on the neck of the cartridge. Measurements from the expended M855 cartridges show good correlation with the predicted plastic deformation of the model. This continuity between the predicted and measured deformation validated the modeling effort.

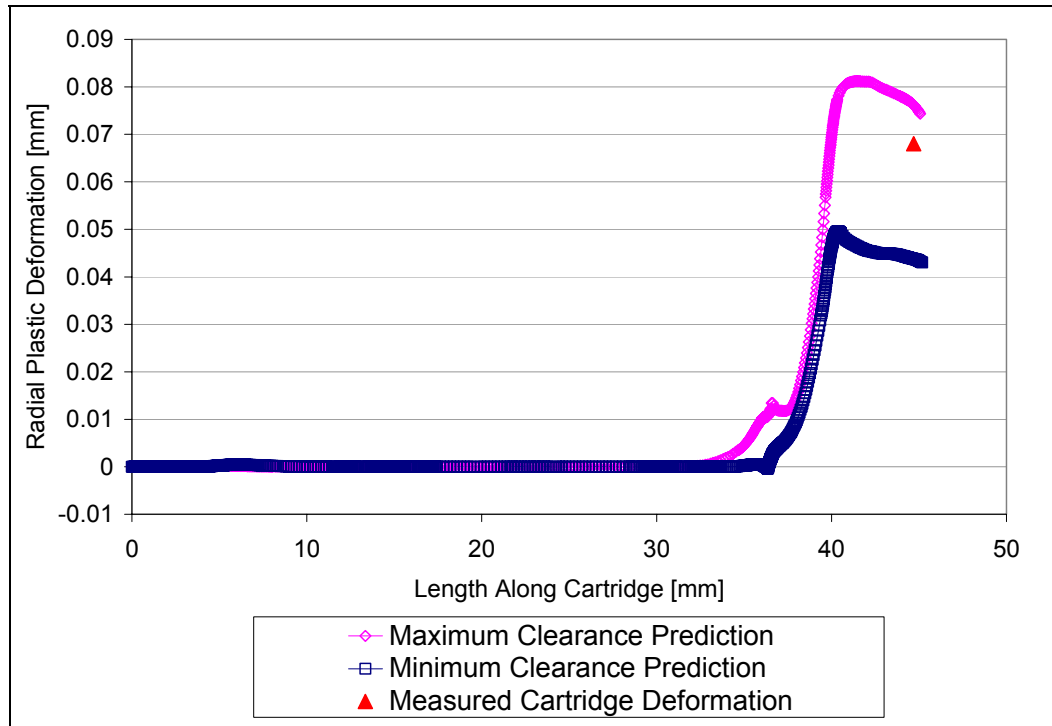


Figure 15. Predicted versus the measured radial plastic deformation along the length of the cartridge.

5. Summary

The over-arching goal of this exercise was to establish a modeling technique for cartridge cases that could be validated against the limited data available during realistic firing conditions. The model generated incorporates the strength changes in the cartridge that result from the variation in the hardness and microstructure produced during manufacturing. The results of the model were used to evaluate the stress, strains, and resulting deformation that a brass cartridge case undergoes during operation. The stress and strain were observed to obey expected trends including expansion and bending of the cartridge to conform to the chamber geometry. The model yielded a stress state within the brass that demonstrated a 1.8 factor of safety. The model was validated with experimental measurements from expended M855 cartridges that showed good correlation with the predicted plastic deformation of the model.

The creation of the validated model serves as a platform from which alternate materials for the cartridge case can be evaluated numerically.

6. References

1. U.S. ARDEC. M855 Cartridge Drawing, Part No. 9378276, Picatinny Arsenal, NJ, 1984.
2. Primer No. 41 Drawing, Part No. 10534280, U.S. Frankford Arsenal: Philadelphia, PA, 1966.
3. Gibbs L.E. Cold Working of Brass, with Special Reference to Cartridge (70-30) Brass. *The American Society for Metals*, Cleveland, OH, 1946.
4. Yang C.J. Bend Ductility of 70-30 Alpha Brass I: Observation. *Materials Science and Engineering* **1989**, *A112*, 1–9.
5. Yang C.J. Bend Ductility of 70-30 Alpha Brass II: Correlation with Tensile Behavior. *Materials Science and Engineering* **1989**, *A112*, 11–20.
6. Hollomon J.H. *Tensile Stress-Strain Curves of a 70-30 Brass*; Memorandum Report 630/7-2; Watertown Arsenal: Watertown, MA, October 1944.
7. Saunders D.S. *The Low Temperature Annealing of 7.62 mm Brass Cartridge Cases: Stress Corrosion Susceptibility*; MRL-R-778; Defence Science and Technology Organisation Materials Research Laboratories: Melbourne, Victoria, 1980.
8. Stehlin, Rick. Data from Olin-Winchester, East Alton, IL, December 2002.
9. Materials Selector 1990, *Materials Engineering*, **December 1989**, 94, Cleveland, OH.
10. U.S. Army Materiel Command. *Engineering Design Handbook, Ammunition Series*, Section 4; Pamphlet AMCP 706-247; Washington, DC, 1964, 160-161.
11. Wagoner R.H. Plastic Behavior of 70/30 Brass Sheet. *Metallurgical Transactions A* **1982**, *13A*, 1941–1500.
12. U.S. ARDEC. Data of M855 Cartridges fired from M16A2, Picatinny Arsenal, NJ, 2002.
13. Corner J. *Theory of the Interior Ballistics of Guns*; John Wiley & Sons Inc.: New York, 282, 1950.
14. U.S. ARDEC. 3-D Technical Data Package for the M16A2, Picatinny Arsenal, NJ, 2003.

NO. OF
COPIES ORGANIZATION

* ADMINISTRATOR
DEFENSE TECHNICAL INFO CTR
ATTN DTIC OCA
8725 JOHN J KINGMAN RD STE 0944
FT BELVOIR VA 22060-6218
*pdf file only

1 DIRECTOR
US ARMY RSCH LABORATORY
ATTN IMNE AD IM DR MAIL & REC MGMT
2800 POWDER MILL RD
ADELPHI MD 20783-1197

1 DIRECTOR
US ARMY RSCH LABORATORY
ATTN AMSRD ARL CI OK TECH LIB
2800 POWDER MILL RD
ADELPHI MD 20783-1197

1 DIRECTOR
US ARMY RESEARCH LAB
ATTN AMSRD ARL SE R H WALLACE
2800 POWDER MILL RD
ADELPHI MD 20783-1197

2 DIRECTOR
US ARMY RESEARCH LAB
ATTN AMSRD ARL SS SE DS R REYZER
R ATKINSON
2800 POWDER MILL RD
ADELPHI MD 20783-1197

7 DIR US ARMY RESEARCH LAB
ATTN AMSRD ARL WM MB M BERMAN
A ABRAHAMIAN M CHOWDHURY
A FRYDMAN T LI W MCINTOSH
E SZYMANSKI
2800 POWDER MILL RD
ADELPHI MD 20783-1197

1 COMMANDER
US ARMY MATERIEL CMD
ATTN AMXMI INT
5001 EISENHOWER AVE
ALEXANDRIA VA 22333-0001

3 CDR US ARMY ARDEC
ATTN AMSTA AR CC M PADGETT
J HEDDERICH H OPAT
PICATINNY ARSENAL NJ 07806-5000

3 CDR US ARMY ARDEC
ATTN AMSTA AR FSA A WARNASH
B MACHAK M CHIEFA
PICATINNY ARSENAL NJ 07806-5000

NO. OF
COPIES ORGANIZATION

6 CDR US ARMY ARDEC
ATTN AMSTA AR CCL F PUZYCKI
R MCHUGH D CONWAY
E JAROSZEWSKI M CLUNE
R SCHLENNER
PICATINNY ARSENAL NJ 07806-5000

3 CDR US ARMY ARDEC
ATTN AMSTA AR CCL A F DINDL
C JOHNSON D WITKOWSKI
PICATINNY ARSENAL NJ 07806-5000

2 CDR US ARMY ARDEC
ATTN AMSTA AR CCL B R MAZESKI
J MIDDLETON
PICATINNY ARSENAL NJ 07806-5000

1 PM MAS
ATTN SFAE AMO MAS
PICATINNY ARSENAL NJ 07806-5000

1 PM MAS
ATTN SFAE AMO MAS
CHIEF ENGINEER
PICATINNY ARSENAL NJ 07806-5000

4 PM MAS
ATTN SFAE AMO MAS MC F HANZL
R KOWALSKI R GULLIFER
G DEROSA
PICATINNY ARSENAL NJ 07806-5000

1 PM MAS
ATTN SFAE AMO MAS PS
PICATINNY ARSENAL NJ 07806-5000

2 PM MAS
ATTN SFAE AMO MAS LC
PICATINNY ARSENAL NJ 07806-5000

2 PM MAS
ATTN SFAE AMO MAS MC
PICATINNY ARSENAL NJ 07806-5000

3 US ARMY TACOM-ARDEC
ATTN AMSTA AR CCI V SCHISSLER
K SPIEGEL R TRAUB
PICATINNY ARSENAL NJ 07806-5000

1 OFC OF NAVAL RESEARCH
ATTN J CHRISTODOULOU
ONR CODE 332
800 N QUINCY ST
ARLINGTON VA 22217-5600

NO. OF
COPIES ORGANIZATION

- 1 NSWG
DAHLGREN DIV CODE G06
DAHLGREN VA 22448
- 1 US ARMY COLD REGIONS
RSCH & ENGRNG LAB
ATTN P DUTTA
72 LYME RD
HANOVER NH 03755
- 3 NASA LANGLEY RESEARCH CTR
ATTN AMSRD ARL VS W ELBER MS 266
F BARTLETT JR MS 266
G FARLEY MS 266
HAMPTON VA 23681-0001
- 2 ALLIANT TECHSYSTEMS
ATTN C CANDLAND R DOHRN
5050 LINCOLN DR
MINNEAPOLIS MN 55436-1097
- 6 ALLIANT TECHSYSTEMS INC
ATTN C AAKHUS MN11 2830
B SEE MN11 2439
N VLAHAKUS MN11 2145
S HAGLUND MN11 2439
M HISSONG MN11 2830
D KAMDAR MN11 2830
600 SECOND ST NE
HOPKINS MN 55343-8367
- 3 AAI CORP
ATTN DR N B MCNELLIS
W ENGEL P SHIPLEY
PO BOX 126
HUNT VALLEY MD 21030-0126
- 4 ARROW TECH ASSOC
ATTN J SEIWERT
1233 SHELBURNE RD STE 8
SOUTH BURLINGTON VT 05403-7700

ABERDEEN PROVING GROUND

- 1 DIRECTOR
US ARMY RSCH LABORATORY
ATTN AMSRD ARL CI OK (TECH LIB)
BLDG 4600
- 3 DIR USARL
ATTN AMSRD ARL SL BB
AMSRD ARL SL BL
AMSRD ARL SL BG
BLDG 328

NO. OF
COPIES ORGANIZATION

- 2 DIR USARL
ATTN AMSRD ARL WM JILL SMITH
J MCCAULEY
BLDG 4600
- 1 DIR USARL
ATTN AMSRD ARL WM B T KOGLER
BLDG 4600
- 1 DIR USARL
ATTN AMSRD ARL WM BA D LYON
BLDG 4600
- 3 DIR USARL
ATTN AMSRD ARL WM BC P PLOSTINS
J NEWILL A ZIELINSKI
BLDG 390
- 3 DIR USARL
ATTN AMSRD ARL WM BD B FORCH
R PESCE-RODRIGUEZ B RICE
BLDG 4600
- 2 DIR USARL
ATTN AMSRD ARL WM BD P CONROY
C LEVERITT
BLDG 390
- 2 DIR USARL
ATTN AMSRD ARL WM BE R LIEB
M LEADORE
BLDG 4600
- 1 DIR USARL
ATTN AMSRD ARL WM BF
S WILKERSON
BLDG 390
- 2 DIR USARL
ATTN AMSRD ARL WM RP J BORNSTEIN
C SHOEMAKER
BLDG 1121
- 1 DIR USARL
ATTN AMSRD ARL WM M B BURNS
J BEATTY
BLDG 4600
- 2 DIR USARL
ATTN AMSRD ARL WM MA S MCKNIGHT
L GHORSE
BLDG 4600

NO. OF
COPIES ORGANIZATION

- 21 DIR USARL
 ATTN AMSRD ARL WM MB B FINK
 J BENDER T BOGETTI
 L BURTON R CARTER
 K CHO W DE ROSSET
 G DEWING R DOWDING
 W DRYSDALE R EMERSON
 D HENRY D HOPKINS
 R KASTE L KECSKES
 B POWERS D SNOHA
 J SOUTH M STAKER
 J SWAB J TZENG
 BLDG 4600
- 7 DIR USARL
 ATTN AMSRD ARL WM MC R BOSSOLI
 S CORNELISON D GRANVILLE
 B HART F PIERCE E RIGAS
 W SPURGEON
 BLDG 4600
- 14 DIR USARL
 ATTN AMSRD ARL WM MD E CHIN
 B CHEESEMAN P DEHMER
 R DOOLEY G GAZONAS
 S GHIORSE M KLUSEWITZ
 J LASALVIA J MONTGOMERY
 W ROY J SANDS S WALSH
 D SPAGNUOLO S WOLF
 BLDG 4600
- 1 DIR USARL
 ATTN AMSRD ARL WM TA W GILLICH
 BLDG 309
- 9 DIR USARL
 ATTN AMSRD ARL WM TA M BURKINS
 B GOOCH T HAVEL C HOPPEL
 E HORWATH T MOYNIHAN
 M NORMANDIA J RUNYEON
 M ZOLTOSKI
 BLDG 393
- 1 DIR USARL
 ATTN AMSRD ARL WM TB P BAKER
 BLDG 309
- 1 DIR USARL
 ATTN AMSRD ARL WM TC R COATES
 W BRUCHEY
 BLDG 309

NO. OF
COPIES ORGANIZATION

- 4 DIR USARL
 ATTN AMSRD ARL WM TD D DANDEKAR
 M RAFTENBERG S SCHOENFELD
 T WEERASOORIYA
 BLDG 4600
- 2 DIR USARL
 ATTN AMSRD ARL WM TE A NIILER
 J POWELL
 BLDG 120